Physica Scripta. Vol. T84, 76–80, 2000

Dynamics, Statistics and Vortex Crystals in the Relaxation of 2D Turbulence

C. F. Driscoll,* D. Z. Jin, D. A. Schecter, E. J. Moreau and D. H. E. Dubin

Physics Department, University of California at San Diego, La Jolla, CA 92093, USA

Received September 6, 1999

PACS Ref: 47.15.Ki, 47.32.Cc, 52.25.Wz, 52.35.Ra, 05.65.+b

Abstract

Magnetically confined electron columns evolve in (r, θ) as essentially inviscid, incompressible 2D fluids with a single sign of vorticity. Turbulent initial states with 50–100 vortices relax due to vortex merger and filamentation, in general agreement with a recent dynamical scaling theory. However, this relaxation sometimes halts when 3–20 vortices "anneal" into a fixed pattern, or "vortex crystal." A new "regional maximum fluid entropy" theory predicts the crystal patterns and background vorticity distribution, by assuming conservation of the robust flow invariants and preservation of the intense vortices. However, simulations show that the character of the relaxed state generally depends strongly on initial conditions and dynamics.

1. Electron plasmas and Euler flows

Magnetically confined pure electron columns are excellent systems for quantitative observations of 2D fluid vortices, turbulence and self-organization [1]. A "generic" experimental apparatus is shown schematically in Fig. 1. The electrons of density $n \sim 10^7$ cm^{-3} are contained within a grounded conducting wall ($2R_w = 7$ cm). A uniform axial magnetic field ($B \lesssim 1$T) provides radial confinement, and negative voltages ($V \lesssim 50$ Volts) applied to end cylinders provide confinement at the ends. The confined plasma is diagnosed and manipulated by antennas on the wall. Finally, the z-integrated electron density $n(r, \theta, t)$ is measured (destructively) by accelerating the electrons onto a phosphor screen and imaging the resulting light with a CCD camera.

The (r, θ) flow of the electrons across the magnetic field occurs due to the strong electric field $\boldsymbol{E}(r, \theta, z) = -\nabla\phi(r, \theta, z)$ from the unneutralized electron plasma. The cross-magnetic-field "drift" velocity is $\boldsymbol{v}(r, \theta, t) = \boldsymbol{E} \times \boldsymbol{B}/B^2$, giving a bulk plasma rotation $f_R(r) \equiv v_\theta(r)/2\pi r \approx 10^4$ s^{-1}. Since the individual electrons move rapidly along the magnetic field lines, electrons behave as rigid "rods" of charge.

In this approximation, the (r, θ) flow of the electrons is described by the 2D drift-Poisson equations [1], which can be written in terms of the vorticity $\zeta(r, \theta, t) \equiv (4\pi|e|c/B)n$ and the scaled electrostatic potential $\psi(r, \theta, t) \equiv (c/B)\phi(r, \theta, t)$ as

$$\frac{\partial \zeta}{\partial t} + \boldsymbol{v} \cdot \nabla\zeta = 0\,, \quad \boldsymbol{v} = -\nabla\psi \times \hat{\boldsymbol{z}},$$
$$\nabla^2\psi = \zeta.$$

These drift-Poisson equations are isomorphic to the Euler Equations. The flow vorticity ζ is proportional to the electron density n, which is directly measured. A column of electrons in vacuum surrounded by a conductor thus evolves as would a 2D vortex in an incompressible inviscid fluid surrounded by a circular *free-slip* boundary. We emphasize that here, there is only one sign of vorticity (taken to be positive), because the density of electrons can only be positive, and there are no charges of opposite sign.

There are also small unwanted diffusive effects due to the end confinement fields [2], and weak "viscous" effects on small spatial scales due to electron-electron collisions [3], but these are *not* modelled by the Euler *or* the Navier-Stokes equation. However, we believe the effects described in this paper do not depend on the details of the fine-scale dissipation.

Euler flows are strongly constrained by integral invariants. The total circulation (number of electrons) $\Gamma_{\rm tot}$, scaled angular momentum P_θ, and scaled electrostatic energy H are well conserved. However, less robust invariants such as the entropy S and enstrophy Z_2 vary significiantly, due to measurement coarse-graining or dissipation of small spatial scales.

2. Waves on a vortex

The simplest stable flow is a centered, symmetric vortex with monotonically decreasing vorticity profile $\zeta(r)$ and azimuthal flow velocity $v_\theta(r)$. Small shape distortions of this nominally symmetric equilibrium can be analyzed as a spectrum of waves with azimuthal and radial mode numbers (m, k), varying as $g_k(r)\exp(im\theta - i\omega_k t)$. These waves are generalizations of the surface distortions on vortex patches referred to as Kelvin waves [4]. Recent analyses have elucidated the process of *inviscid damping* due to wave-fluid interactions at critical radii r_c where $\omega_k/2\pi = mf_R(r_c)$ [5,6], and this damping is routinely observed in electron plasma experiments [7]. These modes have recently been analyzed

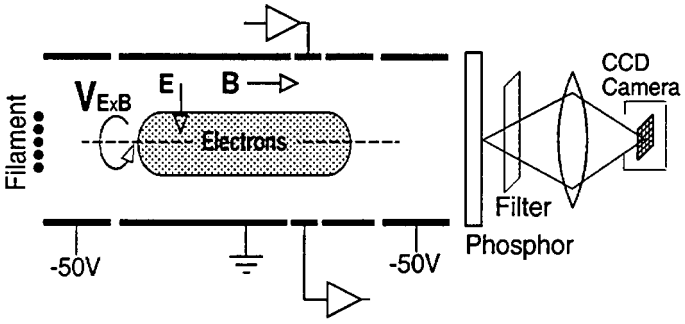

Fig. 1. The cylindrical experimental apparatus with phosphor screen/CCD camera diagnostic.

* e-mail: fdriscoll@ucsd.edu

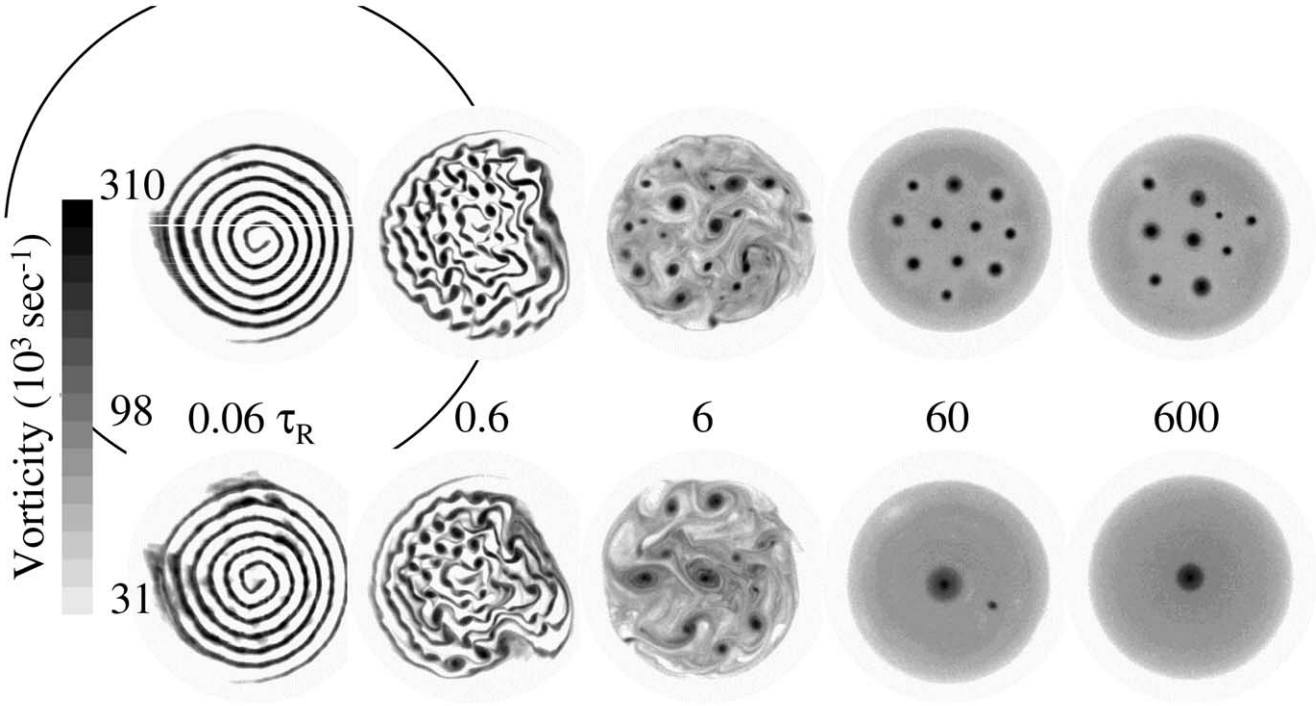

Fig. 2. Images of vorticity at five times for two sequences from similar initial conditions.

in terms of "discrete" and "continuum" eigenfunctions [8,9], with application to atmospheric circulations [9].

For even moderate wave amplitudes, this observed damping is typically nonlinear, and the damping may decrease [6,7] or cease when the resulting "cat's-eye" flows generate fine-scale filaments inside the vortex. For "sharp-edged" vorticity profiles, the resonant radii r_c can be completely outside the vortex, in which case no direct resonance damping occurs. Also, experiments have shown the importance of nonlinear wave-wave couplings: even otherwise stable modes may exhibit "beat-wave damping" [10], whereby energy is observed to flow to longer azimuthal wavelengths.

If the vorticity profile $\zeta(r)$ is "hollow" rather than monotonically decreasing, some of these modes may be unstable, giving the Kelvin-Hemlholtz (shear-flow) instability [11,12]. Both the frequencies and growth rates of these unstable modes are reasonably well characterized by computational solution of the eigenvalue equation using the measured density profiles [13]. One exception is $m = 1$, where we observe a robust exponential instability [14] where cold fluid theory predicts only algebraic growth; here, finite length effects may cause the instability [15,16].

3. Vortex Merger and the Relaxation of Turbulence

The merger of like-sign vortices is fundamental to the relaxation of 2D turbulence at high Reynolds numbers. Experimentally [17], two vortices are observed to merge within a few orbit times when the spacing between vortex centers D is less than 1.6 times the individual vortex diameter $2R_v$; and to orbit without merger for more than 10^4 orbits when $D/2R_v > 1.7$. The merger after 10^4 orbits apparently results from weak non-ideal effects causing R_v to increase, thereby satisfying $D/2R_v < 1.6$. However, the $10^4 : 1$ ratio attests to the weakness of "viscous" effects, and suggests an effective Reynolds number $\mathrm{Re} \approx 10^4 - 10^5$.

Some of the circulation originally trapped in the two individual vortices is "lost" to filamentation; these filaments eventually get stretched and mixed to finer spatial scales than can be imaged, so they form a weak "background" of vorticity.

To study the relaxation of fully developed turbulence, we start with highly filamented initial conditions, which rapidly form many individual vortices, and then freely relax toward a 2D meta-equilibrium [18]. In the initial inviscid relaxation, chaotic mutual advection and vortex merger are clearly important dynamical processes. The final "generic" meta-equilibrium is typically strongly peaked on center, reflecting the single intense vortex resulting from repeated mergers, superimposed on a weaker background vorticity.

Surprisingly, this relaxation is sometimes halted when individual vortices settle into a stable, rotating "vortex crystal" pattern which persists for thousands of rotation times. Figure 2 shows the measured z-averaged electron density $n(r, \theta, t)$ at five times for two slightly different initial conditions: the upper sequence forms vortex crystals, whereas the lower sequence relaxes rapidly to a monotonically-decreasing profile. The observed vortex crystal states consists of 5–20 individual vortices each 4–6 times the background vorticity, arranged in a lattice pattern which rotates with the background.

Figure 3 shows the number of distinct vortices N_v for the two sequences. In each sequence, the unstable filamentary initial condition forms $N_v = 50 - 100$ vortices of roughly equal circulation, after which N_v initially decreases as $N_v \sim t^{-\xi}$. This relaxation is generally consistent with a dynamical Punctuated Scaling Theory based on conserved quantities in repeated vortex merger [19]. The observed ξ range from 0.2 to 1.1 as the initial conditions are varied,

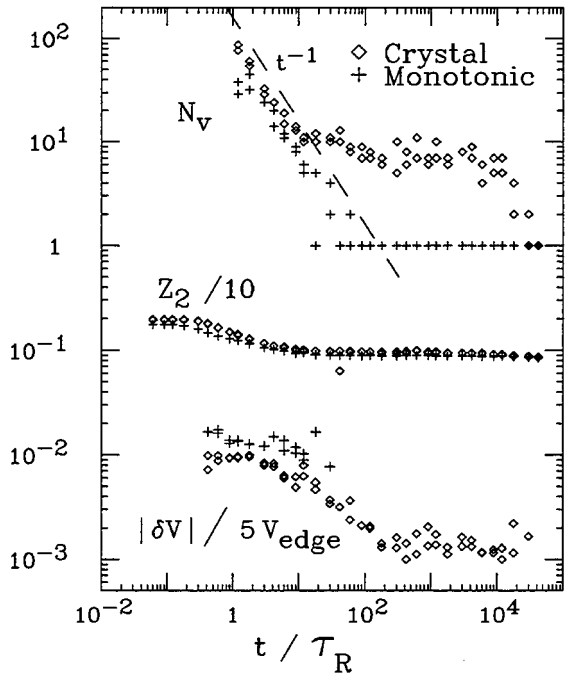

Fig. 3. Number of surviving vortices N_v, the enstrophy Z_2, and the average random velocity $|dV|$.

with 0.8 being commonly observed. In the evolution of the top sequence in Fig. 2, vortex crystals form by $10\tau_R$, and survive for about $10^4\tau_R$. (Here, $\tau_R \equiv 1/f_R(0) = 170\mu s$.) Since the surviving vortices all have about the same circulation, the patterns are quite regular, as seen at $600\tau_R$ in Fig. 2. After $10^4\tau_R$, N_v decreases to 1 as the individual vortices decay away in place due to non-ideal "viscous" effects.

The measured integral quantities for both sequences are consistent with 2D inviscid motion on large scales and dissipation on fine scales. Experimentally, the circulation, angular momentum, and energy are robust invariants. In contrast, the enstrophy Z_2 is a "fragile" invariant, and initially decays a factor of about 2 in both sequences.

Reduction of the chaotic advective motions of the individual vortices is required to form the vortex crystal states. Figure 3 also shows the average magnitude of the random velocities $|\delta V|$ of the individual vortices, with respect to their common rotating frame. The random velocities decrease by a factor of 6 between $2\tau_R$ and $100\tau_R$ for the crystals sequence, whereas only slight cooling is seen before relaxation to $N_v = 1$ for the monotonic sequence. We believe this cooling and cessation of relaxation through mergers is a near-inviscid 2D fluid effect, *i.e.* independent of the details of the fine-scale dissipation. However, the non-zero total circulation is essential: because there is no "negative" vorticity, the diffuse background necessarily persists, and the vortex/background interactions are more pronounced.

In order to show that the cooling of turbulent flow to vortex crystals is a 2D inviscid effect, we have compared the experiments directly to vortex-in-cell simulations with up to 10^6 point vortices [20] to approximate 2D Euler dynamics. The cooling curves are approximately the same in simulation and experiment, and they appear to follow power law decay as $|\delta V| \propto t^{-\alpha}$.

Simulations with different numbers of point vortices have verified that the vortex cooling and crystallization is not sensitive to the discreteness. The point vortex gas is equivalent to an ideal Euler fluid only in the mean field approximation. Microscopic fluctuations of the vorticity about the mean field give rise to "collisional viscosity," and cause distributions of point-vortices to eventually relax to global 2D maximum entropy states.

We believe that cooling occurs through the chaotic mixing of background vorticity by the strong vortices, as opposed to processes such as deformations of individual vortices in the crystal pattern. To test this, we artificially multiply all "background" vorticity by a constant ranging from 0 to 3. Evolving this artificial system forward, we observe cooling which depends on the strength of the background vorticity. There is no cooling in the absence of the background, and there is no cooling if almost all of the circulation is in the background. When the background is too strong, cooling is apparently countered by shears and fluctuations in the background vorticity.

4. Dynamics and entropy

In recent years, two radically different theories have had some success in describing the free relaxation of 2D turbulence. One is the Punctuated Scaling Theory (PST) referred to above [19], which postulates that the turbulent flow is dominated by strong vortices which generally follow Hamiltonian dynamics of point vortices, punctuated by the occasional merger of like-sign vortices. The relaxed state is then one single vortex of each sign, or just one vortex in our case. The PST agrees with the observed power law decrease in the number of strong vortices [18,19], but the theory can not explain why several strong vortices remain and anneal into an equilibrium pattern in the final state of the turbulent relaxation.

A diametrically opposite approach is incorporated in the global maximum fluid entropy (GMFE) theory [21]. This approximates the turbulent flow as a collection of non-overlapping, incompressible microscopic vorticity elements that become ergodically mixed in the relaxed state. Clearly, the GMFE theory can not explain the vortex crystals, since the theory predicts a smooth vorticity distribution.

A new Regional Maximum Fluid Entropy (RMFE) theory approach [22,23] characterizes the vortex crystal states by maximizing the fluid entropy S [21] of the background. The key idea is that some regions of the flow are well-mixed, while other regions are not. The strong vortices ergodically mix the background, driving it into a state of maximum fluid entropy. This mixing, in return, affects the punctuated dynamics of the strong vortices, "cooling" their chaotic motion, and driving them into an equilibrium pattern. However, the vorticity in the strong vortices is trapped and remains unmixed with the background.

The global quantities that determine the RMFE state are the total circulation Γ_{tot}, the angular momentum P_θ, and the energy H. The diffuse background vorticity is assumed to consist of incompressible microscopic vorticity elements of fixed strength ζ_f, with ζ_f taken to be the maximum observed vorticity. Coarse-graining over these randomized vorticity elements then gives the observed background vorticity $\zeta_b(r)$.

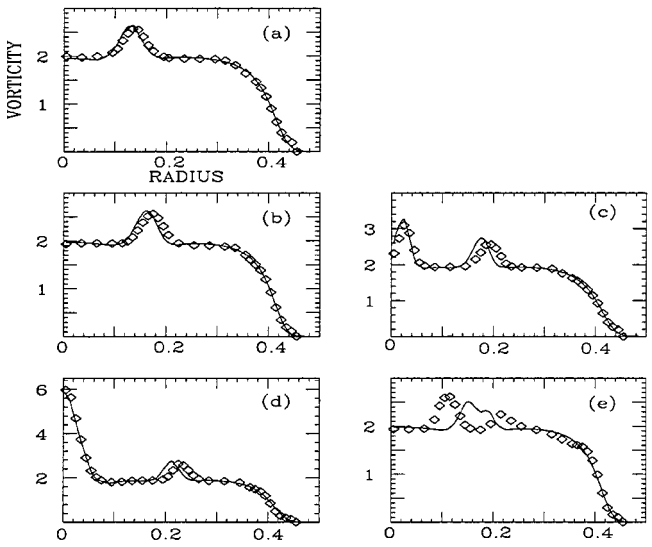

Fig. 4. Measured and predicted theta-averaged vorticity distributions for 5 vortex crystal states.

In addition to the above quantities, the RMFE state depends on the number M of surviving strong vortices and their vorticity distributions $\{\zeta_i(r),\, i = 1, 2 \ldots M\}$. These properties of the strong vortices depend on the details of the early dynamical evolution of the flow, and are beyond the scope of any statistical theory. The statistical theory treats the flow only after the mergers of the strong vortices have ceased.

Given these inputs, two properties of the relaxed vortex crystal state can be predicted: the coarse-grained vorticity distribution of the background $\zeta_b(r)$, and the equilibrium positions $\{\boldsymbol{R}_i\}$ of the strong vortices [22]. The resulting backgrond distributions are of the form

$$\zeta_b(\boldsymbol{r}) \;=\; \zeta_f \;/\; (e^{\beta\zeta_f \Psi} + 1),$$

where $\Psi \equiv \psi + \frac{1}{2}\Omega r^2 + \mu$ is the stream function in the rotating frame, and (β, Ω, μ) are parameters. This "Fermi distribution" occurs because the microscopic vorticity elements are assumed to be incompressible. The RMFE solutions reproduce the observed vortex crystal patterns and background distribution, as can be seen in the $\theta-$averaged vorticity profiles shown in Fig. 4.

Thus, the following physical picture of vortex crystal formation emerges: the strong vortices undergo chaotic mergers described by punctuated scaling theory, but they also ergodically mix the low vorticity background. The mixing of the background, in return, cools the chaotic motion of the vortices, and drives the vortices into a vortex crystal equilibrium. The interaction between the strong vortices and the background, a process neglected in the PST, may be important in understanding the relaxation of 2D turbulence in other situations as well.

Interestingly, recent theory [23] has established estimates for the number of vortices which survive to form the vortex crystal state, by equating the time to merge to the time to cool. Here, the estimates are based on the dynamical scaling exponents ξ and η, which determine the number

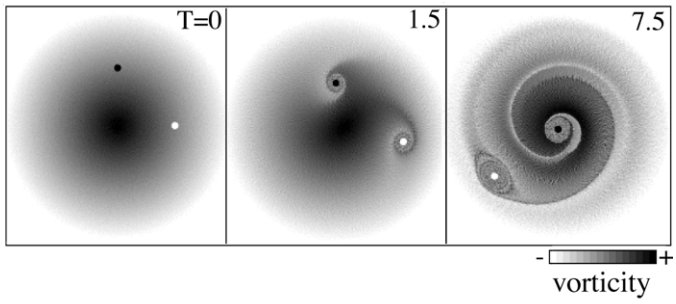

Fig. 5. Gradient-driven radial separation of a clump and hole in a circular shear flow.

of surviving vortices $N_v(t)$ and their total circulation $\Gamma_v(t)$ as

$$N_v(t) = N_v(t_0)\left(\frac{t}{t_0}\right)^{-\xi}, \quad \Gamma_v(t) = \Gamma_v(t_0)\left(\frac{t}{t_0}\right)^{\xi\eta}.$$

Note that the assumptions of PST imply $\eta = 1/2$, but somewhat different values ($0.2 < \eta < 0.8$) are observed in experiments and simulations. The time to merge is given by $1/\tau_m(t) = -(\mathrm{d}/\mathrm{d}t)N_v$, and the cooling time is estimated from mixing arguments as $\tau_c(t) = A/\alpha N_v \Gamma_v$, where A is the area of the vorticity patch, and $\alpha \approx 0.03$. Surprisingly, these simple estimates predict N_c to within about a factor of two.

Other recent theory work has analyzed the dynamics of intense positive vortices (clumps) or negative vortices (holes) on a non-uniform background of (positive) vorticity [24]. The analysis clearly shows that clumps move *up* the vorticity gradient, and holes move *down* the gradient. Figure 5 shows this effect in a numerical simulation used to check the theoretical analysis. The full analysis necessarily treats the flow shear $\partial f_R/\partial r$ separately from the vorticity gradient $\partial\zeta/\partial r$, since they are related only by a spatial integral. The analysis also shows that there can also be stationary self-trapped states for small ratios of $(\partial\zeta/\partial r)/(\partial f_R/\partial r)$.

5. Minimum enstrophy state

Theorists often suggest that relaxed states may be determined from the robust invariants Γ, P_θ, H by either maximization of entropy S [21], or by minimization of the enstrophy Z_2 [25–28], including generalizations thereof [29]. Obviously, the occurrence of vortex crystal states shows that neither principle holds universally.

Nevertheless, early electron plasma experiments found that a range of unstable initial conditions relaxed to near the minimum enstrophy state. Specifically, minimization of enstrophy accurately predicts the meta-equilibrium profiles for hollow initial conditions of moderate energy [30].

These experiments suggested that the relaxed states could indeed be predicted by the robust invariants. However, recent computer simulations starting from unstable annuli of vorticity show that different dynamics and therefore different relaxed states can be obtained from the same invariants [31].

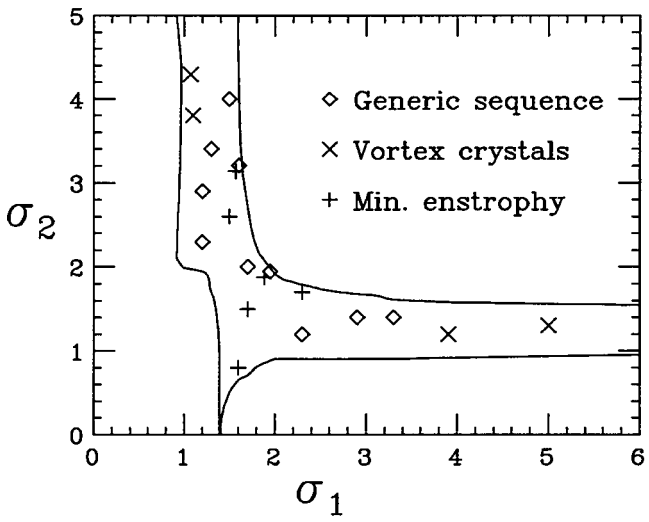

Fig. 6. Types of relaxed states observed in simulations of two annuli with vorticity levels (σ_1, σ_2). Extreme initial vorticity levels lead to persistent strong vortices, giving vortex crystals or generic profiles. Less extreme initial conditions lead to vorticity holes, filamentation, and near-minimum-entropy states.

Specifically, the simulations were started from two annuli of vorticity given by

$$\zeta(r) = \begin{cases} \sigma_1 & \text{for} \quad a_1 < r < b_1 \\ \sigma_2 & \text{for} \quad a_2 < r < b_2 \\ 0 & \text{elsewhere} \end{cases} .$$

The six parameters $\{\sigma_1, a_1, b_1, \sigma_2, a_2, b_2\}$ were chosen subject to fixed $\{\Gamma, P_\theta, H\}$, leaving 3 parameters which were chosen to be $\{\sigma_1, \sigma_2, b_2\}$ for comparison to the experiments. $\{\Gamma, P_\theta, H\}$ were chosen to give $H_{\text{exc}} = 6 \times 10^{-3}$, and b_2 was generally near $0.5\, R_w$. The initial annuli also had a small $m = 1$ or $m = 2$ seed asymmetry.

Figure 6 shows that completely different relaxed states can be obtained, depending on the details of these initial conditions. The relaxed states were characterized as (1) "generic," meaing peaked on center due to complete vortex merger and centerization; (2) "vortex crystals," where the "cooling" process prevented complete merger from occurring; and (3) "minimum enstrophy," where no strong vortices persist, because filamentation dynamics dominated the evolution. We note that the minimum enstrophy profiles are always closer to the minimum enstrophy prediction than to the maximum entropy prediction, suggesting that there may be some validity to Batchelor's inverse cascade hypothesis [28], due to the formation of arbitrarily fine-scale filaments.

Thus, at present, we can only conclude that both dynamics and statistics contribute to the inviscid relaxation of 2D turbulence with a single sign of vorticity.

Acknowledgments

This work was supported by National Science Foundation grant PHY98-76999 and Office of Naval Research grant N00014-96-1-0239.

References

1. Driscoll, C. F. and Fine, K. S., Phys. Fluids **2**, 1359 (1990).
2. Peurrung, A. J. and Fajans, J., Phys. Fluids B **5**, 4295 (1993).
3. Dubin, D. H. E., Phys. Plasmas **5**, 1688 (1998).
4. Kelvin, W., Nature **23**, 45 (1880).
5. Briggs, R. J. *et al.*, Phys. Fluids **13**, 421 (1970).
6. Pillai, N. S. and Gould, R.W., Phys. Rev. Lett. **73**, 2849 (1994).
7. Cass, A. C., Ph.D. dissertation, UCSD (1998).
8. Schecter, D. A., Ph.D. dissertation, UCSD (1999).
9. Montgomery, M. T. and Lu, C., J. Atmos. Sci. **54**, 1868 (1997).
10. Mitchell, T. B., Driscoll, C. F. and Fine, K. S., Phys. Rev. Lett. **73**, 2196 (1994).
11. Levy, R. H., Phys. Fluids **8**, 1288 (1965).
12. Davidson, R. C., "Physics of Nonneutral Plasmas" (Addison-Wesley, New York 1990).
13. Driscoll, C. F. *et al.*, "Plasma Phys Control Nucl Fusion Research **3**, 507 (1988) (Vienna: IAEA 1989).
14. Driscoll, C. F., Phys. Rev. Lett. **64**, 645 (1990).
15. Smith, R. A. and Rosenbluth, M. N., Phys. Rev. Lett. **64**, 649 (1990); Smith, R. A., Phys. Fluids B **4**, 287 (1992).
16. Finn, J., "Compressional Effects in Nonneutral Plasmas, a Shallow Water Analogy and $\ell = 1$ instability" (1999).
17. Fine, K. S., Driscoll, C. F., Malmberg, J. H. and Mitchell, T. B., Phys. Rev. Lett. **67**, 588 (1991).
18. Fine, K. S., Cass, A. C., Flynn, W. G. and Driscoll, C. F., Phys. Rev. Lett. **75**, 3277 (1995).
19. Carnevale, G. F. *et al.*, Phys. Rev. Lett. **66**, 2735 (1991); Weiss, J. B. and McWilliams, J. C., Phys. Fluids A **5**, 608 (1993).
20. Schecter, D. A., Dubin, D. H. E, Fine, K. S. and Driscoll, C. F., Phys. Fluids **11**, 905 (1999).
21. Miller, J., Phys. Rev. Lett. **65**, 2137 (1990); Robert, R. and Sommeria, J., J. Fluid Mech, **229**, 291 (1991); Miller, J., Weichman, J. B. and Cross, M.C., Phys. Rev. A **45**, 2328 (1992), and references therein.
22. Jin, D. Z. and Dubin, D. H. E., Phys. Rev. Lett. **80**, 4434 (1998).
23. Jin, D. Z., Ph.D. dissertation, UCSD (1999).
24. Schecter, D. A. and Dubin, D. H. E., "Vortex Motion Driven by a Background Vorticity Gradient" (1999).
25. Matthaeus, W. H. and Montgomery, D., Ann. N. Y. Acad. Sci. **357**, 203 (1980).
26. Leith, C. E., Phys. Fluids **27**, 1388 (1984).
27. Matthaeus, W. H., Stribling, W. T., Martinez, D., Oughton, S. and Montgomery, D., Phys. Rev. Lett. **66**, 2731 (1991).
28. Batchelor, G. K., J. Fluid Mech. **78**, 129 (1976).
29. Boghosian, B. M., Phys. Rev. E **53**, 4754 (1996).
30. Huang, X.-P. and Driscoll, C.F., Phys. Rev. Lett. **72**, 2187 (1994); Huang, X.-P., Ph.D. dissertation, UCSD (1993).
31. Moreau, E.J. *et al.*, "The Influence of Dynamics on 2D Turbulent Relaxation: A Numerical Study" (1999).